JOURNAL OF AIRCRAFT
Vol. 35, No. 2, March–April 1998

Computation of the Aerodynamic Characteristics of a Subsonic Transport

Lillianne P. Troeger* and Gregory V. Selby†
Old Dominion University, Norfolk, Virginia 23529

An advanced low-order panel method, VSAERO, has been applied to a full-configuration transport aircraft. Wing pressure distributions, as well as lift, drag, and pitching moment coefficients, calculated for the full configuration are compared with experimental data. In addition, the effect of selected vehicle components on aircraft forces and moments was investigated. The results for the complete configuration were compared with those from several partial model configurations. It is shown that the wing-surface pressure distributions and pitching moment coefficient are predicted well by VSAERO. The lift coefficient is consistently overpredicted by the code, as expected for inviscid calculations.

Nomenclature

a = speed of sound
B = fuselage
C_D = drag coefficient, drag/(qS_{ref})
C_L = lift coefficient, drag/(qS_{ref})
C_m = pitching moment coefficient, pitching moment/(qS_{ref}MAC)
C_p = pressure coefficient, $(p - p_\infty)/q$
c = local chord
F = wing fairing
M = freestream Mach number, $a^{-1}(2q/\rho)^{1/2}$
MAC = mean aerodynamic chord, 17.67 in.
p = local static pressure, psf
p_∞ = freestream static pressure, psf
q = dynamic pressure, psf
S_{ref} = reference wing area, 19.92 ft^2
T = tail assembly, including horizontal and vertical tails and associated fairings
W = wing
x, y = streamwise and spanwise distances, respectively
x/c = nondimensional chordwise location
α = angle of attack

Introduction

PANEL methods for aerodynamic applications have been widely used by the aerospace community since the 1960s.[1] Panel methods are presently the only computational tools routinely used in the aerospace industry for the analysis of subsonic and supersonic flow about complex aircraft geometries. One major advantage of panel methods is that they only require a surface panel representation of the geometry. This is a much simpler grid than that required for finite difference or finite element methods. VSAERO is an advanced low-order, three-dimensional panel method that uses piecewise constant source and doublet singularities on flat, quadrilateral surface panels. Panel methods assume inviscid flow. Therefore, differences between experimental and computational data increase as the angle of attack approaches stall, and flow separation begins.

Received Aug. 24, 1996; revision received July 24, 1997; accepted for publication July 28, 1997.

*Department of Mechanical Engineering; currently Graduate Student, Department of Materials Science and Engineering, University of Virginia, Charlottesville, VA 22903. Student Member AIAA.

†Associate Professor, Department of Mechanical Engineering. Senior Member AIAA.

Margason et al.[2] compared five production surface panel methods used to predict the subsonic characteristics of five wing-alone and two wing-body configurations. The codes assessed were HESS, VSAERO, QUADPAN, MCAERO, and PAN AIR; the first three are low-order methods and the latter two are high-order methods. Results were compared on the basis of configuration lift, spanwise load distribution, chordwise pressure distribution, and Mach number effects on lift. It was noted by Margason et al. that VSAERO's calculation of C_L was dependent on the number of spanwise panels, possibly because of insufficient chordwise panel distribution or the details of the treatment in the tip region. The higher-order methods, PAN AIR and MCAERO, provided accurate solutions with fewer panels than the low-order methods. Because the higher-order methods had significantly higher computer execution times and costs, the low-order methods are valuable for parametric studies and iterative calculations. The largest computational configurations in the current investigation involved over 3600 surface panels and over 2000 wake panels and required approximately 4.5 (actual time) for the execution of VSAERO (version E.0) on a Silicon Graphics/IRIS 4D-320 VGX Workstation at NASA Langley Research Center.

The current investigation focused on the generic tactical transport (GTT) model that has been used by the Subsonic Aerodynamics Branch at NASA Langley Research Center as part of the advanced turboprop program. Currently, the program includes propulsion/airframe integration studies utilizing the advanced turboprop (ATP) engine. The GTT was designed as a high-wing, military-type, short takeoff and landing (STOL) subsonic transport. The full, unpowered GTT was numerically modeled in the cruise configuration for various angles of attack and freestream Mach numbers that did not exceed approximately 0.2. The experimental data are compared with computational wing pressure distributions and aerodynamic forces. This undertaking constitutes a code-validation study of VSAERO using wind-tunnel data for the GTT. A validated computational representation of the experimental model allows additional configuration studies to be made without the costly use of a wind tunnel, experimental apparatus, and test personnel.

The effect of selected vehicle components on the aircraft forces and moments was investigated. The results for the complete configuration were compared with those from several partial model configurations. The partial models were obtained by removing the tail, wing fairing, and/or fuselage from the full configuration as shown in Table 1. The partial configurations were analyzed to determine how detailed the actual geometry must be paneled to obtain accurate computational predictions. A simpler configuration requires less effort to panel.

In addition, fewer panels are required, which reduces the computer execution time to obtain computational results.

VSAERO was chosen as the panel method for this investigation for several reasons. As shown in the literature, advanced low-order codes such as VSAERO may be used as engineering design tools with lower computing costs than the higher-order panel methods or Navier–Stokes solvers.[3] The low-order codes produce accuracy similar to that from higher-order methods.[4] VSAERO and several other panel method programs that combine source and doublet singularities have been used extensively enough "as to merit the designation of well-proven design tools."[5] Also, first-order methods such as VSAERO have been shown to satisfactorily model most external flows. Hoeijmakers[4] pointed out that low-order methods model subsonic flows well. The GTT experimental data were obtained at incompressible Mach number conditions. Supersonic flow is better modeled by a higher-order method. An additional motivation for the choice of VSAERO was the fact that low-order panel methods are affected less by the irregular paneling on portions of the surface model of the complex GTT configuration. Finally, VSAERO can be run on a minicomputer, so no mainframe access is required.

Table 1 Computational model configurations

Configuration	Components present
1	$W + B + F + T$
2	$W + B + F$
3	$W + B$
4	W
5	$W + B + T$

Table 2 Number of surface and wake panels for all configurations

Configuration	Patches	Surface panels	Wake panels
WBFT	26	3655	2133
WBF	19	3040	1978
WB	20	2354	2116
W	2	875	1432
WBT	27	2969	2278

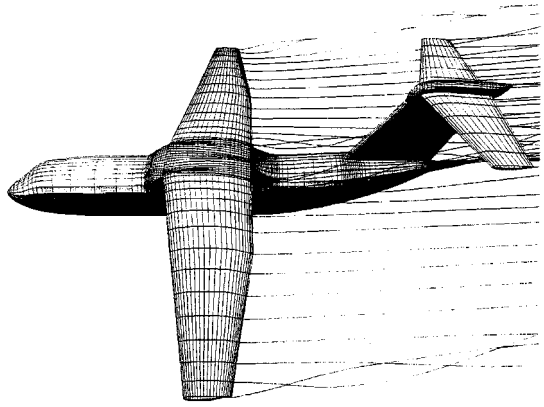

Fig. 1 *WBFT* configuration.

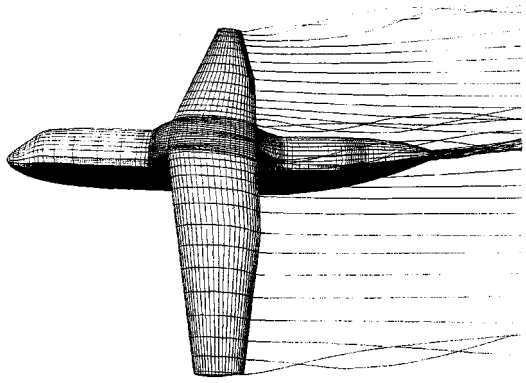

Fig. 2 *WBF* configuration.

Generation of Computational Input Geometry

The surface definition data were processed to obtain a single geometry definition file in VSAERO format. Grids were generated over the entire model using GRIDGEN. Five surface geometries were investigated, as shown in Table 1.

The wake lines were extended approximately seven times the length of the fuselage and divided into 78 wake grid planes. A type-1 wake was shed from each panel along the trailing edges of the wing and horizontal tails. A type-1 wake is one in which the total energy above the wake is equal to that below the wake; i.e., the total pressure is constant across the wake. Static pressure should be equal for any thin wake. A jet wake (vortex-tube) was attached to the aft portion of the fuselage. Table 2 indicates the total number of body surface

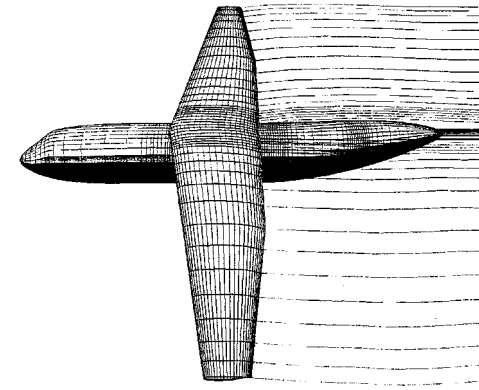

Fig. 3 *WB* configuration.

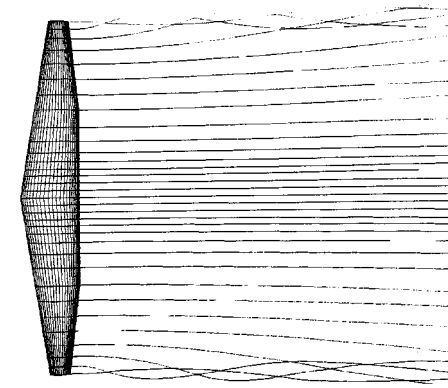

Fig. 4 *W* configuration.

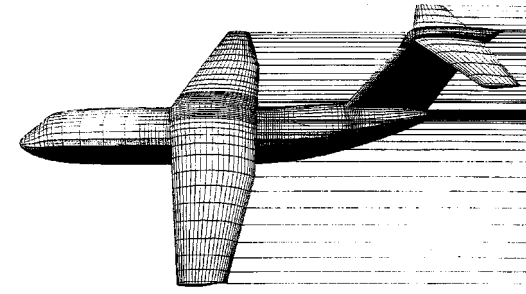

Fig. 5 *WBT* configuration before wake relaxation.

patches and panels, as well as wake panels, used to model each of the configurations. Figures 1–5 show the body mesh representations for the *WBFT*, *WBF*, *WB*, *W*, and *WBT* configurations, respectively.

Description of Experimental Model and Test Facility

The initial phase of GTT model research was to measure and document the aerodynamic characteristics of the unpowered model.[6] The pressure distribution and aerodynamic force data were measured during tests of the GTT in the NASA Langley Research Center's 14- by 22-ft Subsonic Tunnel. Applin et al.[6] provided a database of wing-surface pressure distributions for various model configurations and freestream flow conditions. This database may be used to validate high-lift system analytical tools. A sketch of the experimental GTT model is shown in Fig. 6.

The wing of the GTT had five chordwise rows of pressure taps as shown in Fig. 7. The three inboard chordwise stations were positioned close to the engine nacelle location. The fourth chordwise station was located near the midspan of the outboard flap. The outboard pressure-tap station was located near the middle of the aileron.

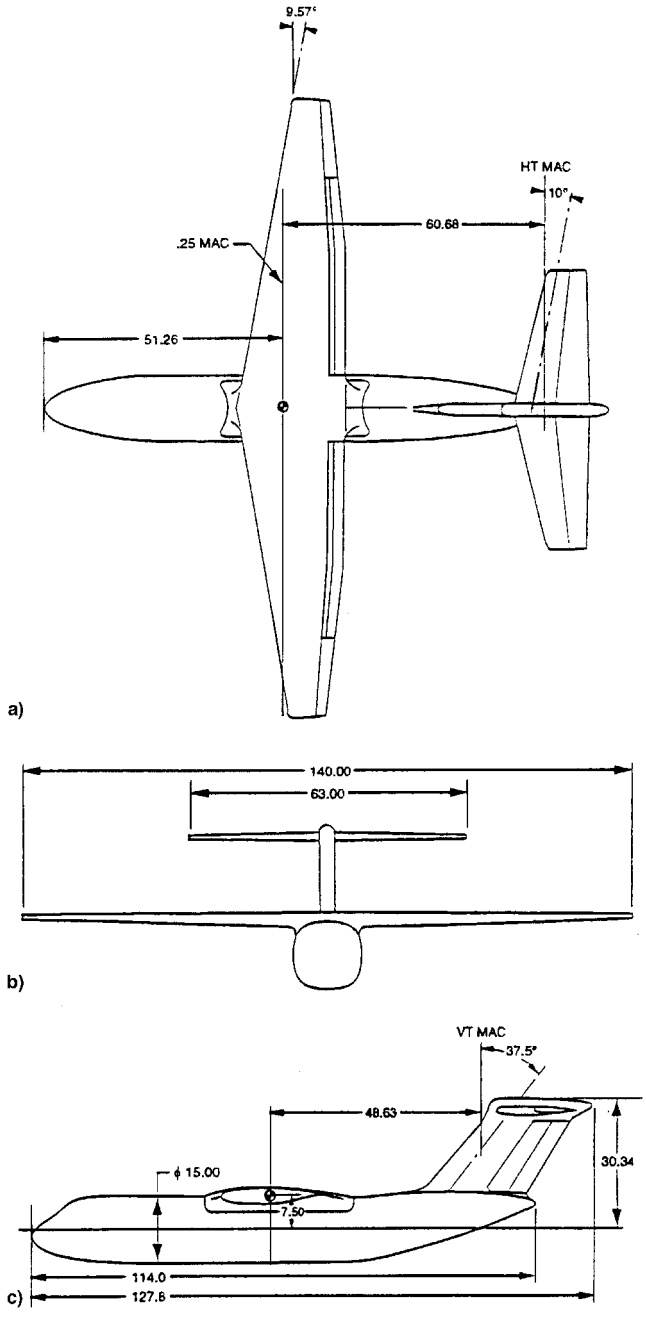

Fig. 6 GTT model: a) top, b) front, and c) side views.

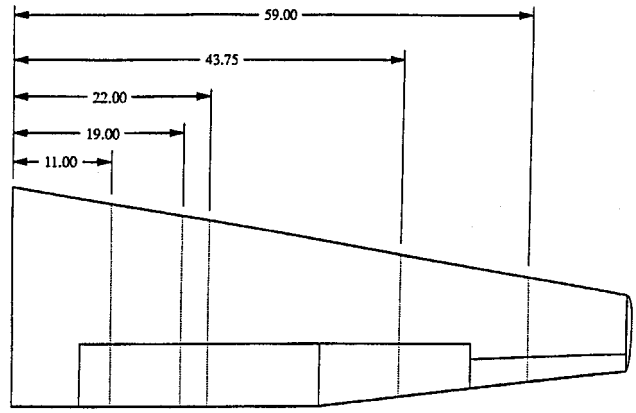

Fig. 7 Location of pressure-tap stations on the wing of the experimental model.

The test matrix for the unpowered GTT included angles of attack from −4 to 22 deg and sideslip angles of 0 and ±15 deg. In some cases, model oscillations prevented the achievement of the highest angles of attack. Various trailing-edge flap deflections and one Krueger deflection schedule were investigated at freestream dynamic pressures q of 20, 40, and 60 psf. These dynamic pressures correspond to freestream Mach numbers of approximately 0.12, 0.16, and 0.2, respectively.[6] The tests of primary interest for the current investigation involved the cruise wing configuration; i.e., zero flap and Krueger deflection. Applin et al.[6] applied wind-tunnel jet boundary corrections and wing, body, and wake blockage corrections to the data as prescribed by Herriot.[7] No corrections were made to the data because of tunnel flow angularity or support system interference.

Results and Discussion

Comparison Between Experimental and Computational Data

Computational results were obtained by executing VSAERO (version E.0) using a Silicon Graphics/IRIS 4D-320 VGX workstation. Surface pressure distributions obtained using VSAERO for the *WBFT* configuration for all q values and at angles of attack of 0 and 14 deg are presented in Figs. 8–10 for data at spanwise semispan stations of 11.0, 22.0, and 59.0 in., respectively. As expected, these figures indicate that the variation in q had little effect on the computational pressure distributions. Therefore, all pressure distributions presented for the configurations discussed herein are for q = 40 psf only, because it was the median value investigated.

The pressure distributions obtained for the *WBFT* (full) configuration compared with experimental data are presented in Figs. 11–15 for all spanwise locations. Good agreement exists between experimental and computational data for the leading-edge region of the wing, with discrepancies noted for the trailing-edge region. VSAERO increasingly overpredicted the suction peaks for $y \geq 19.0$ in. (stations progressing outboard), with errors ranging from 6.25% at y = 19.0 in. to 29% at y = 59.0 in., but underpredicted the suction peak for y = 11.0 in. The increase in suction peak with increasing semispan location, for both experimental and computational data, is consistent with the performance of unswept, tapered-wing planforms, for which lift-induced α increases toward the wing tip. The station at y = 11.0 in. was closest to the wing fairing and body and, therefore, most subject to wing/body interference effects. Interference effects such as at the wing/body junction were not considered in the current computations. Wing-tip effects were not apparent because the current computational and experimental results were compared up to 84% semispan.

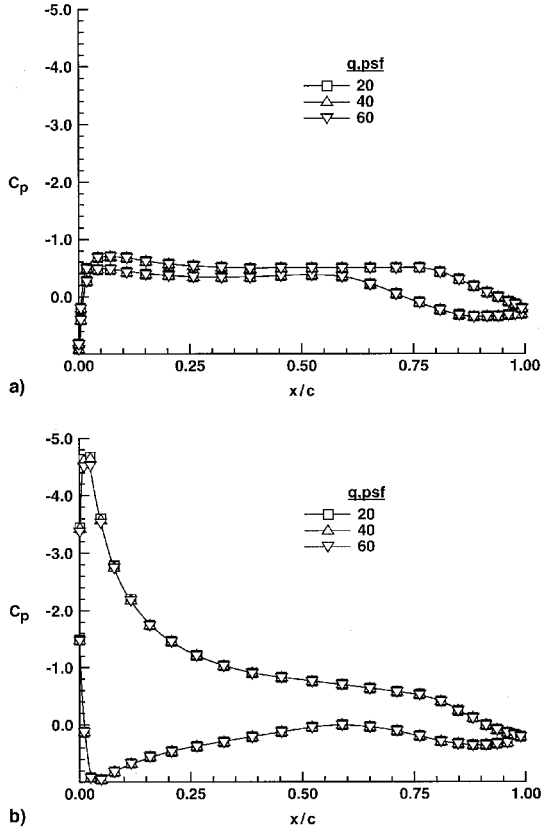

Fig. 8 Computational pressure distributions for the *WBFT* configuration for all q values at y = 11.0 in. α = a) 0 and b) 14 deg.

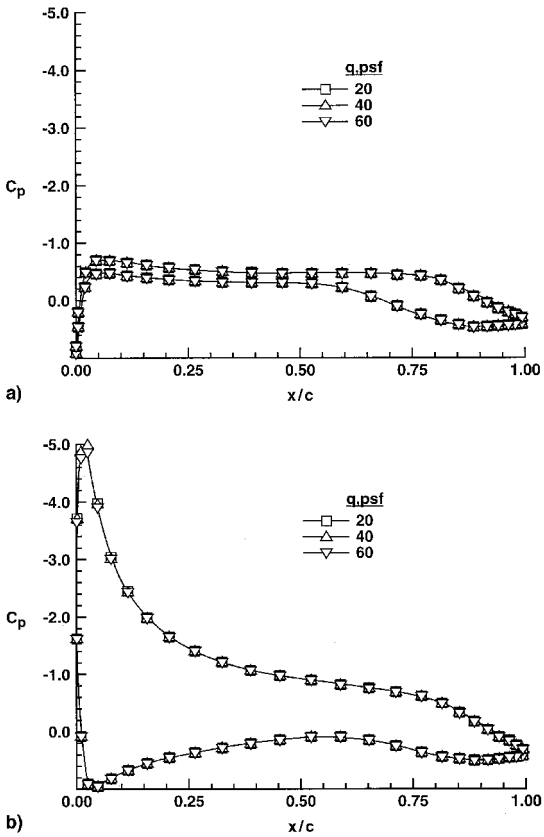

Fig. 9 Computational pressure distributions for the *WBFT* configuration for all q values at y = 22.0 in. α = a) 0 and b) 14 deg.

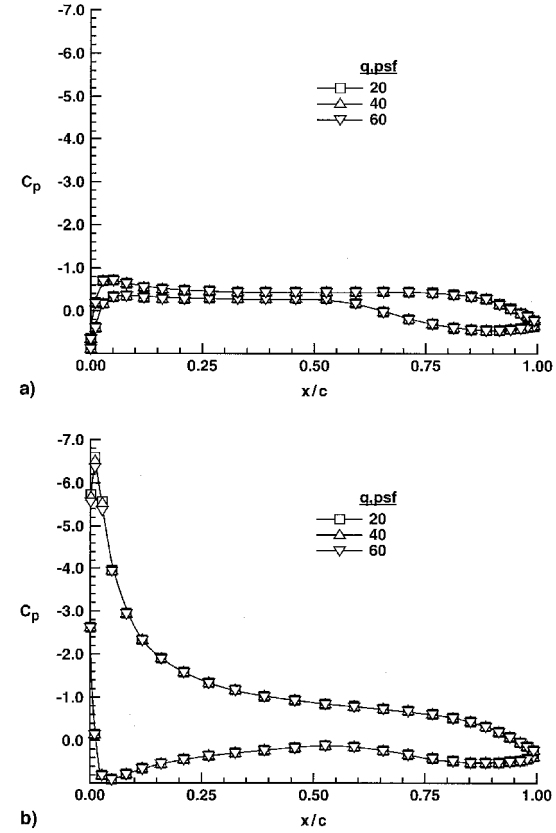

Fig. 10 Computational pressure distributions for the *WBFT* configuration for all q values at y = 59.0 in. α = a) 0 and b) 14 deg.

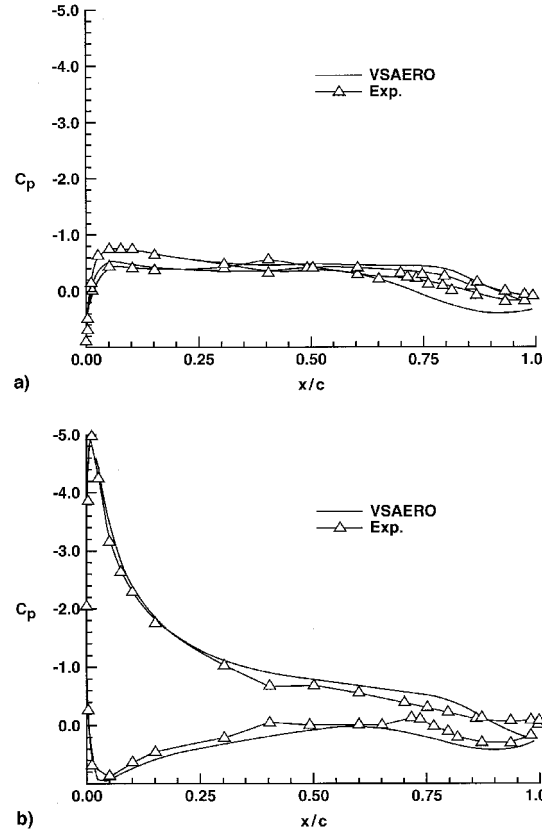

Fig. 11 Computational and experimental pressure distributions for the *WBFT* configuration for q = 40 psf at y = 11.0 in. α = a) 0 and b) 14 deg.

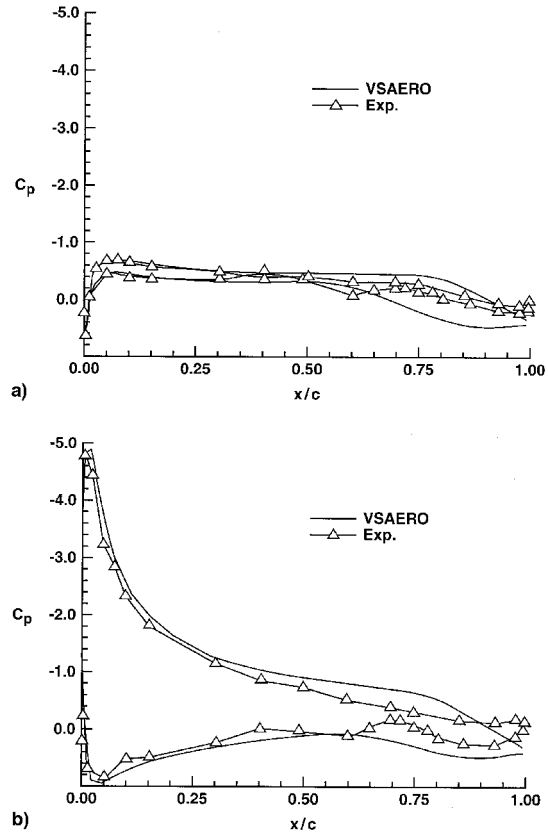

Fig. 12 Computational and experimental pressure distributions for the *WBFT* configuration for q = 40 psf at y = 19.0 in. α = a) 0 and b) 14 deg.

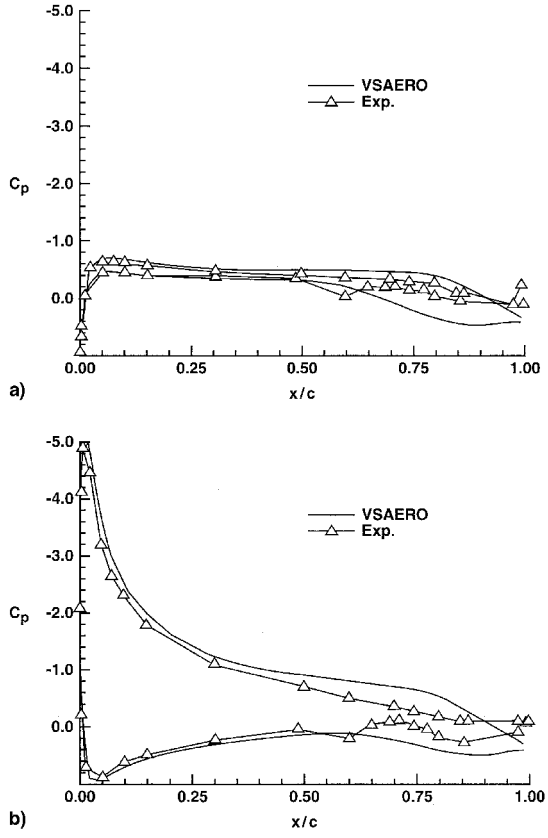

Fig. 13 Computational and experimental pressure distributions for the *WBFT* configuration for q = 40 psf at y = 22.0 in. α = a) 0 and b) 14 deg.

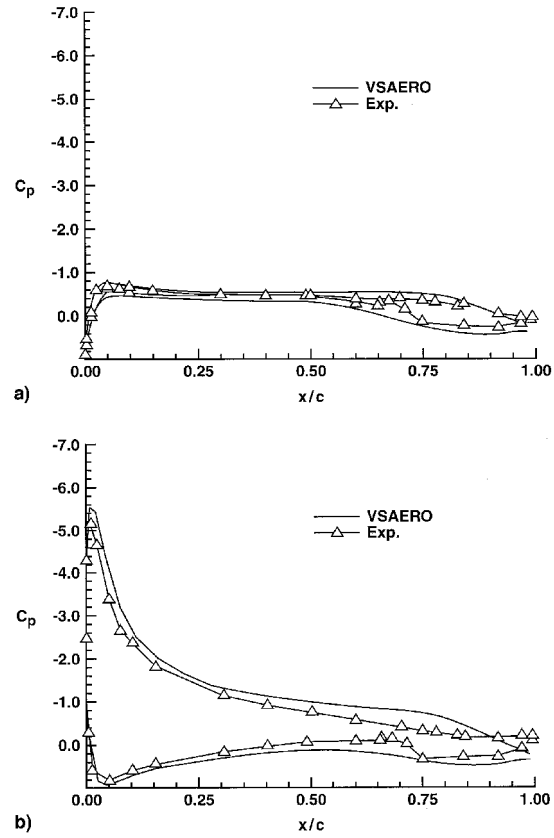

Fig. 14 Computational and experimental pressure distributions for the *WBFT* configuration for q = 40 psf at y = 43.75 in. α = a) 0 and b) 14 deg.

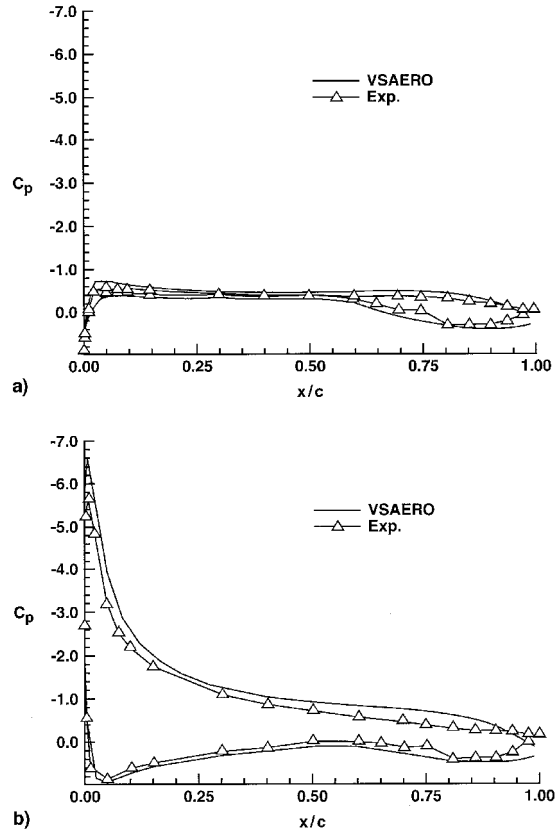

Fig. 15 Computational and experimental pressure distributions for the *WBFT* configuration for q = 40 psf at y = 59.0 in. α = a) 0 and b) 14 deg.

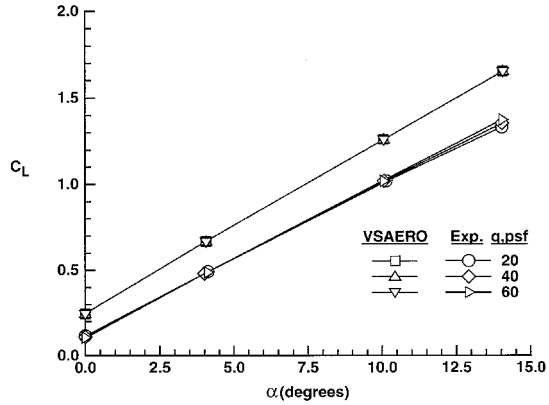

Fig. 16 Computational and experimental lift coefficients vs angle of attack for the *WBFT* configuration for all q values.

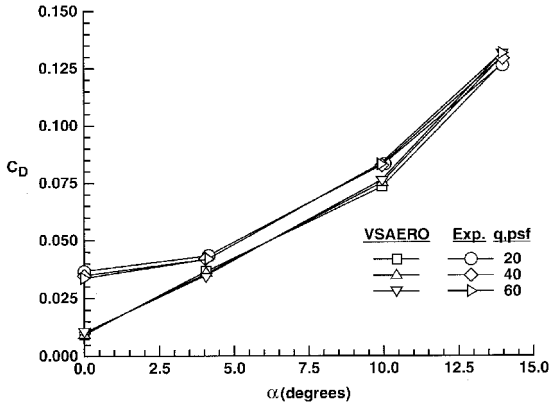

Fig. 17 Computational and experimental drag coefficients vs angle of attack for the *WBFT* configuration for all q values.

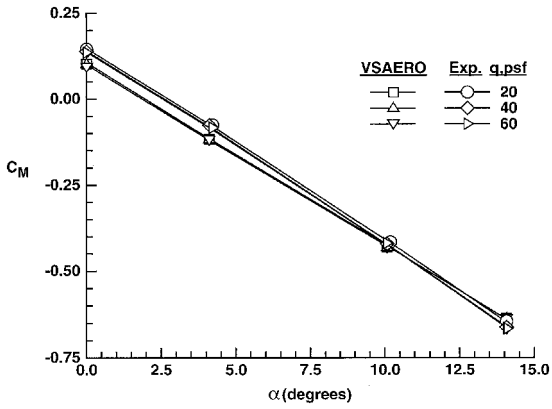

Fig. 18 Computational and experimental pitching moment coefficients vs angle of attack for the *WBFT* configuration for all q values.

Discrepancies between the experimental and computational pressure distributions were primarily caused by viscous effects. Experimentally, the leading edge of the wing was smooth and continuous. Flow over such a surface would not be dominated by the viscous effects; therefore, an inviscid code such as VSAERO should model flow in the leading-edge region well, which it did, as seen in Figs. 11–15. However, the downstream portion of the wing on the experimental model contained gaps, steps, and flap-track fairings associated with the double-slotted trailing-edge flap system present for $11.0 \leq y \leq 43.75$ in. and the aileron at $y = 59.0$ in. The presence of these surface discontinuities increased the viscous effects in the downstream region of the wing, which would not be properly predicted by an inviscid code. Local disturbances such as the presence of tape on the model or inaccurate pressure taps are also possible sources of discrepancies at individual data points. Also, the sharp cusp present at the trailing edge of the experimental wing was difficult to model computationally; therefore, it is possible that the experimental and computational geometries did not match at the trailing edges.

The major differences between the experimental pressure data and the computational results near the trailing edge are likely caused by separation on the experimental wing. The GTT experienced a gradual trailing-edge stall beginning near the middle of the range of angles of attack investigated, characterized by movement of the separated (stalled) region toward the leading edge. A near-zero slope of the upper-surface C_p distribution near the trailing edge indicates flow separation. For a 14-deg angle of attack, separated flow progresses from $x/c \approx 0.8$ to 0.9. VSAERO assumed that the flow was attached over the entire surface, because it was specified that separation occurred only at the trailing edge.

The experimental and computational aerodynamic force and moment coefficients as functions of α are compared for all values of q in Figs. 16–18. These figures reinforce the lack of effect of variations in q on the results. In Fig. 16, it is seen that VSAERO overpredicted the lift coefficient by 35–100% for lift coefficients from 1.4 to 0.1. This is consistent with the findings of Margason et al.[2] The intersection of the lift curves with the negative α axis indicates an effective $\Delta\alpha \approx 1.5$ deg (at $C_L = 0$). It is likely that this difference is caused by several effects. Local differences in α between the computational and experimental models might have been because of geometrical differences or an error in setting α for the experimental model. In addition, viscous flow effectively increases airfoil thickness with increasing chordwise position, which reduces camber and lift. Also, viscous flow thickens the airfoil trailing edge, which reduces the downwash angle and lift. The lift curves are

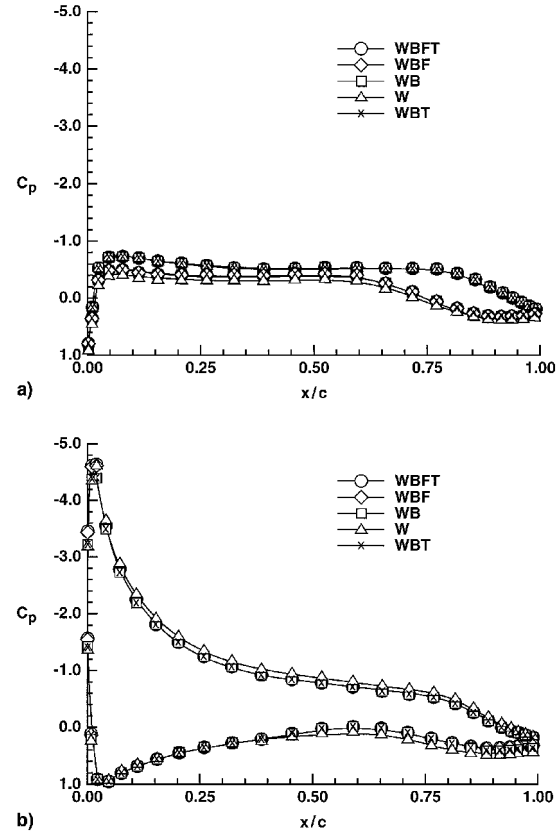

Fig. 19 Computational pressure distributions for all configurations for q = 40 psf at y = 11.0 in. α = a) 0 and b) 14 deg.

slightly divergent. This is expected from pressure losses on the experimental model due to trailing-edge separation, which is not accounted for computationally. VSAERO's boundary-layer function was not used. Hence, the computations assumed that viscous effects were negligible and that flow was attached over the entire wing, resulting in greater lift.

Drag coefficient as a function of angle of attack is presented in Fig. 17. Computational and experimental drag coefficient data display good agreement for $\alpha \geq 4$ deg. It should be noted, however, that computational values of C_D only account for induced drag (profile drag is not considered because VSAERO assumes inviscid flow).

Figure 18 depicts the relationship of moment coefficient to angle of attack. (Positive pitching moment is nose up.) The line formed by the computational data has a lower slope than the experimental curve, but, overall, the agreement with experiments is good. A possible source of error between the computational and experimental pitching-moment coefficients was inaccurate specification of the moment center in the reduction of the experimental force data.

Comparison of Computational Configurations

The purpose of the five computational configurations was to determine to what extent the geometry of the experimental (*WBFT*) configuration must be represented computationally to give accurate predictions of surface pressure distributions and lift, drag, and pitching moment coefficients. Figures 19–21 show the pressure distributions for the five computational configurations at y = 11.0, 22.0, and 59.0 in., respectively, for angles of attack of 0 and 14 deg. Results are shown for q = 40 psf only. The wing pressure distributions for the five computational configurations were nearly coincident. The most appreciable differences occurred for the wing-only configuration at y = 11.0 in. The wing-only configuration experienced a slightly increased pressure coefficient on the lower surface for $\alpha \leq 4$ deg, in addition to increased suction on the upper surface for $\alpha \geq 10$ deg. This trend was most likely because of the slight difference in the inboard geometry for the wing-only configuration. The *WBT* configuration produced a slightly higher suction peak than the other configurations for α = 14 deg beginning at $y \geq 43.75$ in.

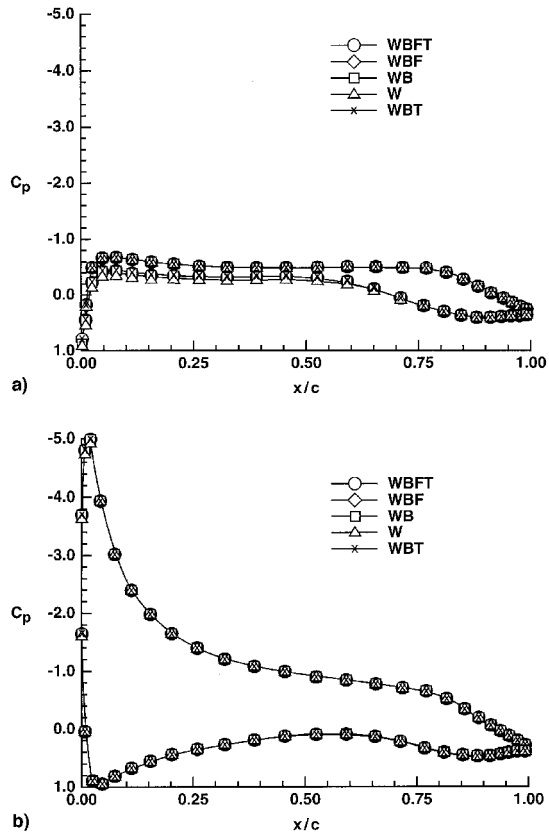

Fig. 20 Computational pressure distributions for all configurations for q = 40 psf at y = 22.0 in. α = a) 0 and b) 14 deg.

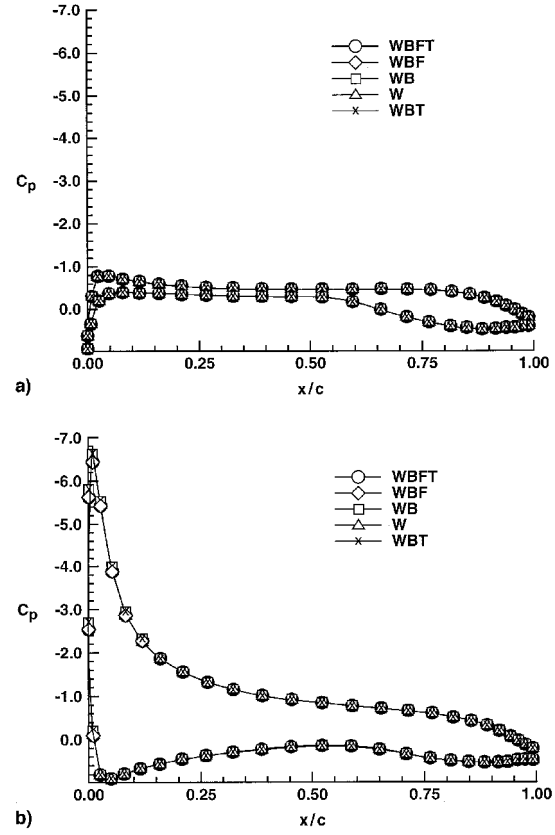

Fig. 21 Computational pressure distributions for all configurations for q = 40 psf at y = 59.0 in. α = a) 0 and b) 14 deg.

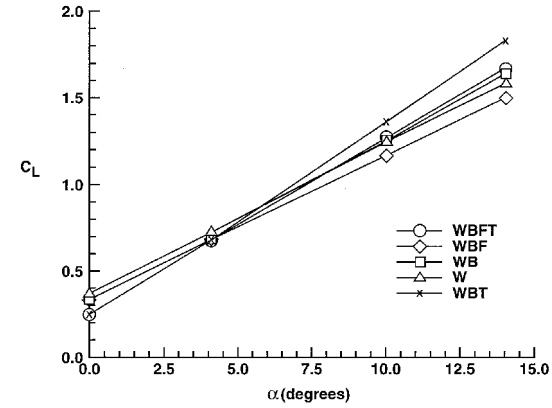

Fig. 22 Computational lift coefficient vs angle of attack for all configurations for q = 40 psf.

The lift curves for the five configurations are shown in Fig. 22. The *WBT* configuration produced the highest lift-curve slope, whereas the *WBF* produced the lowest slope. The *WB* and *W* configurations induced similar lift-curve slopes. A comparison of C_L data for the *WBFT* and *WBT* configurations indicates that the presence of the wing fairing decreases the lift-curve slope (≈5 to 10% reduction at the highest α). This conclusion also applies to the comparison of C_L data for *WBF* and *WB* configurations. As a result of viscous flow effects (not modeled by VSAERO), a significant change in C_D would be expected, but not in C_L.

Conclusions

VSAERO was used to obtain wing pressure distributions for the full configuration of the GTT model with good results. The code tended to overpredict the suction pressures on the upper wing surface and underpredict on the lower surface, mainly for the trailing-edge portion of the wing in both cases. The code overpredicted the lift coefficient, as expected for an inviscid code, but modeled the lift-curve slope well. The trend for the drag coefficient as a function of angle of attack was predicted accurately for $\alpha \geq 4$ deg. The pitching moment was predicted accurately for nearly all angles of attack. It was shown that the value of q had little effect on the computational and experimental results.

The wing-surface pressure distributions for the five computational configurations were predicted well by VSAERO. There were slight discrepancies for the wing-only configuration at the inboard station. The *WBT* configuration produced the highest predicted lift-curve slope, followed by the *WBFT*; However, the overall trends were not greatly divergent.

The purpose of the five computational configurations was to determine to what extent the geometry of the experimental (*WBFT*) configuration must be represented computationally to give accurate predictions of surface pressure distributions and lift, drag, and pitching moment coefficients. The results herein show that the geometrically complex wing fairing did not need to be included to give accurate wing pressure distributions. In fact, only the wing needs to be modeled if the region of interest is fairly well removed from areas of potential wing/body interference. The addition of the fairing made a significant difference in the calculation of the lift coefficient.

Acknowledgment

The authors are grateful for the support of the NASA Graduate Researchers Program and the Virginia Space Grant Consortium. The authors thank Z. T. Applin for helpful discussions concerning experimental models and data.

References

[1]Schippers, H., "On the Evaluation of Aerodynamic Influence Coefficients," *Notes on Numerical Fluid Mechanics, Volume 21: Panel Methods in Fluid Mechanics with Emphasis on Aerodynamics, Proceedings of the 3rd GAMM Seminar* (Kiel, Germany), 1987, pp. 210–218.

[2]Margason, R. J., Kjelgaard, S. O., Sellers, W. L., III, Morris, C. E. K., Jr., Walkey, K. B., and Shields, E. W., "Subsonic Panel Methods—A Comparison of Several Production Codes," AIAA Paper 85-0280, Jan. 1985.

[3]Maskew, B., "Prediction of Subsonic Aerodynamic Characteristics—A Case for Low-Order Panel Methods," AIAA Paper 81-0252, Jan. 1981.

[4]Hoeijmakers, J. W. M., "Panel Methods in Aerodynamics," *Notes on Numerical Fluid Mechanics, Volume 21: Panel Methods in Fluid Mechanics with Emphasis on Aerodynamics, Proceedings of the 3rd GAMM Seminar* (Kiel, Germany), 1987, pp. 1–34.

[5]Henne, P. A., *Applied Computational Aerodynamics*, Vol. 125, Progress in Astronautics and Aeronautics, AIAA, Washington, DC, 1990.

[6]Applin, Z. T., Gentry, G. L., Jr., and Takallu, M. A., "Wing Pressure Distributions from Subsonic Tests of a High-Wing Transport Model," NASA TM-4583, Jan. 1995.

[7]Herriot, J. G., "Blockage Corrections for Three-Dimensional-Flow Closed-Throat Wind Tunnels, with Consideration of the Effects of Compressibility," NACA Rept. 995, 1950.